Multiple ionization of Ar by F^- impact: Projectile-electron-loss and direct-ionization collision channels

M. M. Sant'Anna,* F. Zappa, A. C. F. Santos, L. F. S. Coelho, W. Wolff, A. L. F. de Barros, and N. V. de Castro Faria
Instituto de Física, Universidade Federal do Rio de Janeiro, Cx. Postal 68528, Rio de Janeiro 21941-972, Brazil
(Received 31 May 2006; published 1 August 2006)

We have measured single- and multiple-target ionization cross sections for the F^-+Ar collision system. Measurements of the final target and projectile charge states were performed in coincidence, separating the collision channels for single-, double-, and triple-projectile-electron loss and for direct ionization. The studied velocity region extends from $v=0.46$ to $v=1.45$ atomic units. Results are compared with existing H^-+Ar data as well as with Ar multiple ionization by protons, electrons, and antiprotons. For the direct-ionization channel, ratios for multiple-to-single target ionization are similar to those found for H^++Ar collisions. For this channel multiple ionization is well described by independent single-ionization events by a frozen projectile. For the projectile-electron-loss collision channels, on the other hand, the correlation between projectile electrons and target electrons plays an important role. Our data show that the average final charge state of the target, $\langle q \rangle$, increases steeply with the final charge state of the projectile, while an independent-particle model (neglecting two-center electron-electron correlation) only accounts for small variations of $\langle q \rangle$.

DOI: 10.1103/PhysRevA.74.022701 PACS number(s): 34.50.Fa

I. INTRODUCTION

The high degree of electronic correlation in negative ions makes the description of their electronic structures a difficult task. Nevertheless, considerable progress in this field has been achieved. As the recent reviews by Andersen [1] and Pegg [2] show, this was done both experimentally, with a plethora of very precise data on the spectroscopy of anions being obtained using electron beams, lasers, and synchrotron radiation, and theoretically, with refined many-body theories. The study of collisions between anions and multielectron targets, on the other hand, has advanced more slowly and still is a very challenging theoretical problem. This is not surprising as describing the collision dynamics, including ionization processes, for multielectronic projectiles and targets is a tough task even for positive or neutral projectiles, where the electronic structures are easy to compute (e.g., [3–8]). Such a description is even harder for negative-ion projectiles, where in addition one has to cope with much more complex wave functions.

Irrespective of the projectile charge state, experimental cross-section data for simultaneous target and projectile multiple ionization are needed to shed light on atomic collision processes, but their availability is small for positive projectiles and almost nil for anionic projectiles [9–11]. Structureless projectiles are a special but instructive case, with fewer collision channels and, for example, the study of multiple ionization of noble gases by protons provided plenty of information on the many ionization pathways leading to a certain final target charge state [12,13]. In particular there are two competing mechanisms: (a) direct multiple outer-shell ionization and (b) inner-shell ionization followed by Auger relaxation, with relative weights that depend on the collision system and final target charge state, respectively dominating at intermediate and high velocity collisions. A similar behavior was verified with antiprotons [14,15]. Considering now atomic projectiles with electronic structure, the electrons add in complexity to the problem, particularly for negative-ion projectiles. The projectile electrons can play quite different roles, depending on the collision channel, and henceforth comparison between anionic and structureless projectiles will contribute to clarify the problem.

Multiple ionization of atoms by anions, besides its basic importance in the physics of collisions, does occur in nature and their cross sections are important parameters for modeling several atmospheric and technological applications. One example is the use of high-velocity H^- beams as a starting point for producing high-velocity neutral hydrogen beams, a well-known strategy for plasma heating in magnetically controlled fusion devices [16]. More recently, negative heavy-ion beams have been proposed as drivers for inertial confinement fusion, as high-velocity neutral projectiles produced by photodetachment may efficiently impact and heat up a hydrogen pellet target in a fusion chamber [17,18]. Detailed charge-changing cross sections are consequently needed to estimate the beam attenuation in the residual gases [18,19].

In the present work, we report on coincidence measurements of Ar multiple ionization by F^- projectiles in the 0.46–1.45 velocity range [atomic units (a.u.) are used for velocities throughout the paper]. To our knowledge, the only other anion-argon collision system with charge-state coincidence cross sections available in the literature is the H^-+Ar for velocities between 4.47 and 8.94 a.u. [10]. There are, however, electron detachment and target excitation studies for fluorine anions colliding with noble gases, employing electron-photon and electron-projectile coincidence techniques [20,21], but without recording the final target charge state and at very low velocities ($v \leqslant 0.2$ a.u.) where target ionization is unlikely.

In short, we have measured cross sections $\sigma^{p,q}$ for the collision channels

*Electronic address: mms@if.ufrj.br

TABLE I. Multiple ionization of Ar by F^- ions: cross sections for single-projectile-electron loss with target ionization (10^{-18} cm^2).

E (keV)	Ar^+	Ar^{2+}	Ar^{3+}	Ar^{4+}
100	25 ± 5	3.7 ± 0.8	0.40 ± 0.08	
200	52 ± 11	13 ± 3	1.6 ± 0.4	
300	69 ± 14	21 ± 5	3.3 ± 0.7	0.20 ± 0.08
400	70 ± 14	24 ± 5	5.2 ± 1.0	0.30 ± 0.12
500	77 ± 16	26 ± 6	5.4 ± 1.1	0.90 ± 0.36
600	82 ± 17	31 ± 7	8.4 ± 1.7	0.60 ± 0.24
700	89 ± 18	32 ± 7	8.7 ± 1.7	0.50 ± 0.20
800	99 ± 20	35 ± 7	11.2 ± 2.3	1.4 ± 0.6
900	102 ± 21	31 ± 7	8.2 ± 1.7	09 ± 0.6
1000	113 ± 23	38 ± 8	10.5 ± 2.1	0.9 ± 0.6

$$F^- + Ar \rightarrow F^p + Ar^q + (p+q+1)e^-, \quad (1)$$

with $p=-1$ (direct target ionization), $p=0$ (single-projectile-electron loss), $p=1$ (double-projectile-electron loss), and $p=2$ (triple-projectile-electron loss). Regarding the target ionization, final Ar charge states up to $q=4$ were measured.

The single and multiple ionization of Ar by F^- show, for the direct-ionization collision channel, the same cross-section proportions observed for H^++Ar equivelocity collisions. For the projectile-electron-loss collision channels, however, the analysis of our data shows a different situation. There is the correlation between the average number of target electrons ionized and the number of electrons lost by the projectile. This effect is stronger than would be expected for collisions without a direct dynamical correlation between projectile electrons and target electrons, with the measured electron emission cross sections obeying a binomial distribution.

This article is organized as follows. Section II describes the experimental setup used in the coincidence experiments. In Sec. II we also present the measured cross sections for direct ionization and projectile electron loss in coincidence with the final target charge state. In Sec. III, we compare our results to Ar multiple-ionization data obtained with H^- and with structureless projectiles. Possible mechanisms for the creation of multiply charged Ar ions are discussed. In Sec. IV, a summary and some conclusions are presented.

II. EXPERIMENT AND RESULTS

The experiment was performed at the Universidade Federal do Rio de Janeiro (UFRJ), using a 1.7-MV tandem accelerator from National Electrostatics Company. Details about the experimental setup were published elsewhere [22], and only the main features are discussed here.

The accelerator is equipped with a negative-ion source, based on the sputtering of material from a sample containing the element of interest. In order to obtain F^- ions in the range of hundreds of keV, the tandem accelerator is used in a configuration slightly different from the usual. The low-energy anions produced in the ion source are accelerated up to the high-voltage potential at the center of the accelerator. In collisions within a gas stripper part of the beam is neutralized. The F^0 beam crosses the second tandem stage without additional acceleration. A second gas cell is used at the exit of the accelerator to produce the high-energy F^- ions in electron-capture collisions.

TABLE II. Multiple ionization of Ar by F^- ions: cross sections for double-projectile-electron loss with target ionization (10^{-18} cm^2).

E (keV)	Ar^+	Ar^{2+}	Ar^{3+}	Ar^{4+}
200	7.0 ± 2.1	4.1 ± 1.3	1.1 ± 0.4	0.10 ± 0.04
300	16 ± 5	9.3 ± 2.8	2.5 ± 0.8	0.20 ± 0.08
400	8.1 ± 2.5	11 ± 4	6.1 ± 1.9	0.60 ± 0.24
500	32 ± 10	22 ± 7	8.3 ± 2.5	0.80 ± 0.32
600	54 ± 17	46 ± 14	16 ± 5	1.6 ± 0.7
700	42 ± 9	35 ± 7	14 ± 3	2.1 ± 0.9
800	54 ± 11	43 ± 9	18 ± 4	2.6 ± 1.1
900	57 ± 12	47 ± 10	21 ± 5	2.9 ± 1.2
1000	64 ± 13	56 ± 12	28 ± 6	3.6 ± 1.5

The resulting high-energy F^- beam is deflected by a switching magnet towards the collision chamber and crosses the argon jet, placed in front of a time-of-flight system. The emerging beam exiting the collision chamber is charge analyzed by a parallel-plate deflector and detected in a second chamber placed 2 m apart from the first one. Each projectile particle hits a biased aluminum plate, ejecting secondary electrons which are detected by a channeltron. The coincident detection of the argon recoil ions and the fluorine projectiles allows one to obtain the desired cross sections. Data were normalized by previous measurements of Ar ionization by protons at 1.0 MeV [23]. An independent check for the normalization procedure, using data for Ar ionization by C^{3+} ions at 2.0 MeV [24], agreed within 10% with the proton normalization.

Our results for multiple ionization of Ar by F^- ions [Eq. (1)] are presented in Tables I–IV and Fig. 1. Figure 1(a) shows cross sections for single-projectile-electron loss with target ionization $\sigma^{0,q}$ as a function of projectile energy (q is the target final charge state). Data with q values going from 1 up to 4 are shown, using squares for single ($q=1$), circles

TABLE III. Multiple ionization of Ar by F^- ions: cross sections for triple-projectile-electron loss with target ionization (10^{-18} cm^2).

E (keV)	Ar^+	Ar^{2+}	Ar^{3+}	Ar^{4+}
200	0.29 ± 0.06	0.80 ± 0.16	0.45 ± 0.09	0.05 ± 0.02
300	0.74 ± 0.15	1.1 ± 0.3	0.70 ± 0.14	0.11 ± 0.05
400	0.92 ± 0.19	2.3 ± 0.5	3.0 ± 0.6	0.86 ± 0.35
500	2.4 ± 0.5	4.1 ± 0.9	2.9 ± 0.6	0.50 ± 0.20
600	3.9 ± 0.8	6.1 ± 1.3	3.7 ± 0.8	0.93 ± 0.38
700	5.3 ± 1.1	8.0 ± 1.6	6.8 ± 1.4	1.8 ± 0.8
800	7.3 ± 1.5	12.2 ± 2.5	10.4 ± 2.1	2.3 ± 0.9
900	7.9 ± 1.6	15.2 ± 3.1	11.9 ± 2.4	3.4 ± 1.4
1000	11.2 ± 2.3	21.2 ± 4.3	17.5 ± 3.5	4.0 ± 1.6

TABLE IV. Multiple ionization of Ar by F^- ions: cross sections for target direct ionization (10^{-18} cm^2). For this collision channel there is no projectile electron loss.

E (keV)	Ar^+	Ar^{2+}	Ar^{3+}
100	22 ± 7	5.2 ± 2.1	
200	24 ± 8	6.8 ± 2.8	
300	18 ± 6	4.3 ± 1.8	
400	23 ± 5	4.2 ± 1.7	
500	27 ± 6	4.2 ± 1.7	
600	26 ± 6	4.9 ± 1.5	
700	33 ± 7	4.3 ± 0.9	
800	35 ± 7	4.6 ± 1.0	
900	37 ± 8	4.0 ± 1.2	
1000	45 ± 9	5.7 ± 1.2	0.62 ± 19

for double (q=2), up triangles for triple (q=3), and down triangles for quadruple target ionization (q=4). Figure 1(b) shows double-projectile-electron loss $\sigma^{1,q}$, Fig. 1(c) shows triple-projectile-electron loss $\sigma^{3,q}$, and Fig. 1(d) shows direct target ionization $\sigma^{-1,q}$ (the four figures use the same symbol notation for the target final charge states).

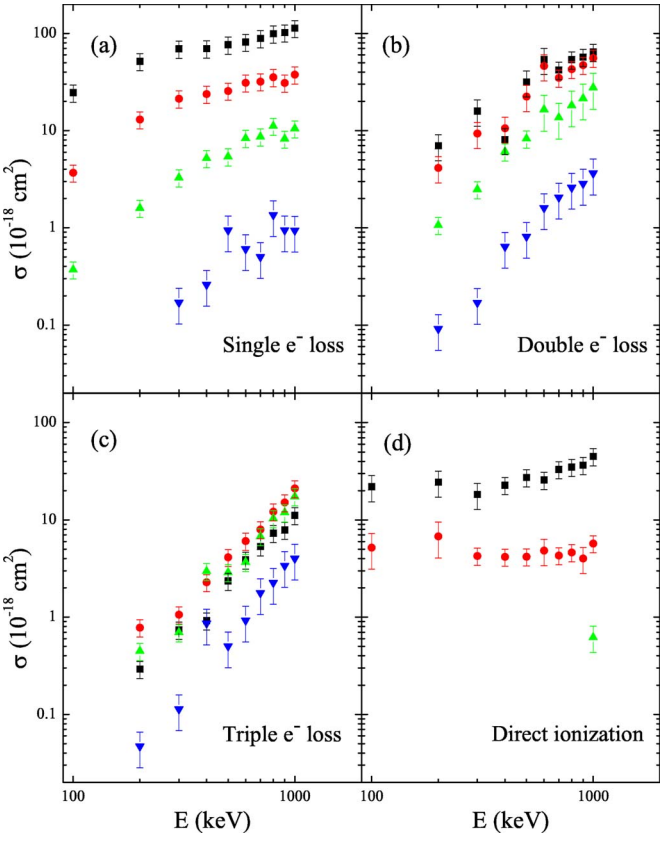

FIG. 1. (Color online) Cross sections for multiple Ar ionization as a function of the projectile energy: squares, single ionization; circles, double ionization; triangles, triple ionization; down triangles, quadruple ionization. Different projectile collision channels are shown in different blocks: (a) Single-electron loss, (b) double-electron loss, (c) triple-electron loss, and (d) direct target ionization.

TABLE V. Cross sections for F^- total direct ionization by incident neutral Ar (10^{-17} cm^2). For this collision channel there is no Ar ionization.

E (keV)	σ_s (10^{-17} cm^2)
43	52 ± 13
76	55 ± 10
100	60 ± 6
200	82 ± 9
300	92 ± 11
400	94 ± 11
500	89 ± 11
600	82 ± 12
700	83 ± 13
800	76 ± 12
900	74 ± 12
1000	67 ± 13

Our coincidence measurements alone do not directly provide information about the collision channels for which the target remains neutral. In such a case the target does not feel the electric field applied by the extraction grids and is, therefore, not detected. However, complementary measurements, using the beam-attenuation technique [22], can be combined with our data to separate the total projectile-electron-loss cross sections with and without target ionization. The beam-attenuation technique allows the determination of the total projectile destruction cross section σ_d corresponding to the sum of single- and all multiple-projectile-electron-loss collision channels, regardless of the target final charge state:

$$\sigma_d = \sum_{p>-1} \sum_{q} \sigma^{p,q}, \tag{2}$$

with q summed from 0 to the number of electrons in the projectile. The collision channel for which the projectile loses one or more electrons and the target remains neutral (q=0) is therefore included in those measurements. The corresponding cross section σ_s can be obtained through the subtraction

$$\sigma_s = \sigma_d - \sum_{p>-1} \sum_{q>0} \sigma^{p,q}. \tag{3}$$

In the projectile frame of reference, σ_s is the cross section for total direct ionization of the negative ion F^- by the neutral projectile Ar. Alternatively, using the target frame of reference, it is often analyzed as the so-called screening projectile electron loss, as will be discussed in the following section. Cross section values for σ_s are shown in Table V.

III. DISCUSSION

Experimental cross-section data available in the literature for systems involving anions are very scarce. Regarding the argon target, to our knowledge, the only available coincidence-charge-state measurements are for high-velocity H^- projectiles [10]. A comparison of these literature results

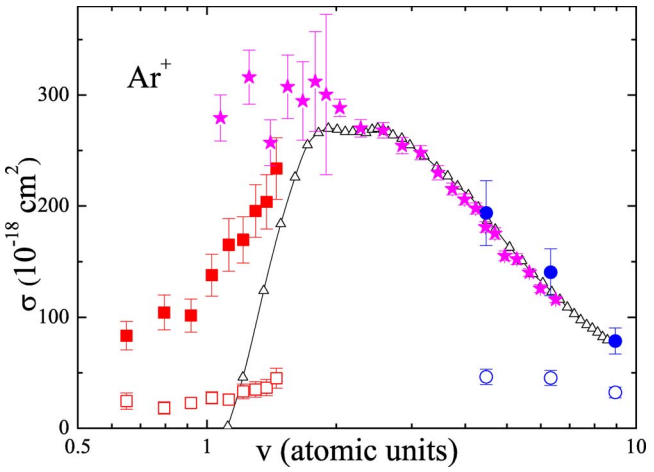

FIG. 2. (Color online) Cross sections for the production of Ar^+ as a function of the projectile velocity: open triangles, electron-impact ionization [25]; open squares, direct ionization by F^-, this work; open circles, direct ionization by H^- [10]; solid squares, total Ar^+ production by F^-, this work [Eq. (4)]; solid circles, total Ar^+ production by H^- [10] [Eq. (4)]; stars, total Ar^+ production by antiprotons [15].

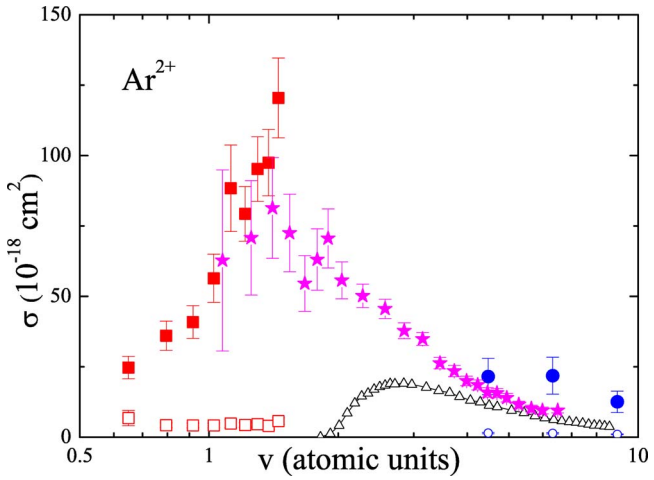

FIG. 3. (Color online) Cross sections for the production of Ar^{2+} as a function of the projectile velocity: open triangles, electron-impact ionization [25]; open squares, direct ionization by F^-, this work; open circles, direct ionization by H^- [10]; solid squares, total Ar^{2+} production by F^-, this work [Eq. (5)]; solid circles, total Ar^{2+} production by H^- [10] [Eq. (5)]; stars, total Ar^{2+} production by antiprotons [15].

with our F^-+Ar intermediate-velocity data is not straightforward. However, data for electron-impact ionization of Ar offer a connection between the two sets of data and shed light on the multiple-ionization processes involved. Argon multiple ionization by protons and antiprotons also pave the way for our analysis.

It is convenient to open the discussion with the target single ionization. Figure 2 shows two sets of cross-section values measured in this work: the direct-ionization (no projectile electron loss, open squares) and the total (irrespective of electron loss, solid squares) values. The figure also shows electron-impact cross sections for single Ar ionization (open triangles) [25] and H^-+Ar direct-ionization cross-section values (open circles) [10], with the latter being much lower than the former, the e^-+Ar direct-ionization cross section. This may seem unexpected at first sight, since it is well known that the single ionizations of Ar by equivelocity electrons and protons are almost identical at these high velocities [14]. Nevertheless, one has to keep in mind that anions are weakly bound if compared to atoms. The ionization of the atomic target may lead to a large probability of a simultaneous ionization of the projectile. For each impact parameter, the sum of probabilities for concurring collision channels is limited to 1. Therefore, a very strong channel will partially inhibit other channels. Thus, one possible explanation for the low-$\sigma^{-1,1}$ cross-section values is that the direct-ionization channel is coupled to a strong projectile-electron-loss channel. This analysis is reinforced as Fig. 2 shows a remarkable agreement between electron-impact data (open triangles) and the high-velocity total Ar^+ production by H^- (solid circles):

$$\sigma_{Ar^+} = \sum_p \sigma^{p,1}, \tag{4}$$

with p running from -1 to 1. This similarity indicates that the anionic projectile ionizes the target just like a point charge. In the course of this collision the projectiles are often also ionized but only the charge of the incoming projectile seems to be relevant, and not the relative yield for the several possibilities of the outgoing projectile (H^-, H^0, and H^+).

A similar situation arises at low velocities, where electron-impact data (open triangles) also differ significantly from equivelocity F^-+Ar direct-ionization data (open squares) in Fig. 2, presenting a better agreement with F^-+Ar total data. Electron-impact data present an energy threshold due to the first Ar ionization potential, while the F^- direct-ionization data increase slightly with velocity but do not show this behavior. The σ_{Ar^+} (solid squares), obtained for F^-+Ar [from Eq. (4) with p summed from -1 to 2], show once more a resemblance to the single ionization Ar by electron impact (open triangles). For the projectile electron loss, the weakly bound anion electron behaves as a quasifree electron and an energy threshold shows up smoothed, due to the momentum distribution probability for the projectile electrons [26,27]. The velocity trend of the σ_{Ar^+} cross sections for F^-+Ar suggests a merging with the electron-impact data around the maximum of the electron impact curve. Data for total single ionization of Ar by antiprotons [15] are also shown in Fig. 2 (stars). Antiprotons are heavy compared to electrons and do not show the velocity threshold around $v=1$, highlighting in Fig. 2 the threshold behavior of the F^- data. The above comparisons lead to a picture consistent with a dominant F^-+Ar collision channel for which the correlation between projectile electrons and target electrons plays a decisive role. This two-center electron-electron correlation will be discussed later in this section.

Double target ionization presents a quite different picture from single target ionization, as can be seen when comparing Figs. 2 and 3. In Fig. 3 we see that, although the relative behaviors of the high-velocity H^- and the low-velocity F^- data are the same as in the previous figure, electron-impact

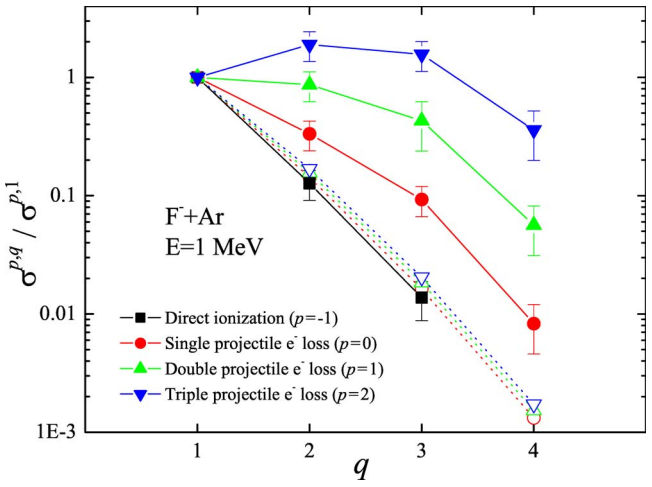

FIG. 4. (Color online) Ratios of multiple- to single-ionization cross sections of Ar by 1-MeV F^- ions as a function of the final target charge state (this work). Solid symbols are used for experimental data and open symbols for results obtained from fitting described in the text: squares, direct ionization; circles, single-projectile-electron loss; triangles, double-projectile-electron loss; down triangles, triple-projectile-electron loss. Lines are just guides to the eye.

data are rather different from the total H^- and F^- data. Cross sections for high-velocity total Ar^{2+} production by H^- (solid circles),

$$\sigma_{Ar^{2+}} = \sum_p \sigma^{p,2}, \tag{5}$$

with p running from -1 to 1, are larger than the electron-impact data (open triangles). However, it is for the F^- projectile (open or solid squares) that the difference to electron-impact data is more extreme. All of our F^- data are below the double-ionization electron-impact threshold and nevertheless our $\sigma_{Ar^{2+}}$ measured total cross sections [obtained for F^- + Ar from Eq. (5) summed over p from -1 to 2] are up to one order of magnitude larger than the maximum electron-impact double-ionization cross section. The same situation holds, qualitatively, for triple and quadruple Ar ionization by the F^- projectiles, with some degree of correlation between projectile and target final charge states. Antiproton projectiles [15] (stars), being heavy, do not present the double-ionization threshold either. In the overlapping region with our total double-ionization data (Fig. 3) antiprotons and F^- data agree within the experimental errors.

Figure 4 compares, for 1 MeV (v=1.45 a.u.) F^-, the ratios $\sigma^{p,q}/\sigma^{p,1}$. For any fixed q (the number of target electrons ionized) the ratios increase with p (the parameter $p+1$ is the number of electrons lost by the projectile). Thus, there is an enhancement of multiple target ionization when more projectile electrons are lost. There are at least two factors leading to this enhancement: (i) correlation exclusively via a common dependence on the collision impact parameter b for target ionization by the projectile and for the (otherwise independent) projectile ionization by the target [5–8,28] and (ii) two-center electron-electron correlation, directly involving at least one pair of electrons, with one electron located at the projectile and the other one located at the target. For both (i) and (ii) the multielectronic character of the projectile and target is essential. We proceed in the analysis of these two factors.

A detailed theoretical description of the studied collisions involving the correlation between the many-projectile electrons and the many-target electrons is beyond the scope of this work. We instead model the collisions neglecting two-center electron-electron correlation and show that an independent electron approximation (IEA) [26] is not efficient to describe simultaneous projectile and target ionization, except for the direct ionization collision channel.

In an impact parameter formulation the cross section for ionizing n out of N equivalent target electrons and m out of M equivalent projectile electron is given by

$$\sigma_{m,n}^{(M,N)} = \int P_{m,n}^{(M,N)}(b) 2\pi b db. \tag{6}$$

Considering target and projectile ionization as independent events the probability integrated in Eq. (6) can be approximated by the product of probabilities

$$P_{m,n}^{(M,N)}(b) = P_m^{(M)}(b) P_n^{(N)}(b). \tag{7}$$

Within the binomial version of the IEA [26] we have

$$P_m^{(M)}(b) = \binom{M}{m} p_p(b)^m [1 - p_p(b)]^{M-m} \tag{8}$$

as the probability for ionizing m among the M outer-shell projectile electrons and

$$P_n^{(N)}(b) = \binom{N}{n} p_t(b)^n [1 - p_t(b)]^{N-n} \tag{9}$$

as the probability for ionizing n among the N outer-shell target electrons. The functions $p_p(b)$ and $p_t(b)$ are, respectively, the probabilities for ionizing a single electron from the projectile and from the target, while the other electrons are frozen. For the F^-+Ar system, the final projectile charge state p is equal to $m+1$ and the final target charge state q is equal to n. Simple Gaussian functions were used for projectile and target single-electron ionizing probabilities: $p_p(b) = p_p(0)\exp(-b^2/R_p^2)$ and $p_t(b) = p_t(0)\exp(-b^2/R_t^2)$. The adjusted fitting parameters, at 1 MeV, are $R_t = 1.45a_0$, $R_p = 3.41a_0$, $p_t(0) = 0.0828$, and $p_p(0) = 0.106$. The Hartree-Fock calculations [29] for the $3p$ electron of Ar result in $\langle r \rangle = 1.66a_0$, close to our value for R_t. Our R_p value is about twice the R_t value. This relation is consistent with a binding energy for F^-, 3.399 eV, much smaller than the Ar binding energy, 15.76 eV. Exponential probabilities were also tested with no significative changes in the fitting results. Gaussian probabilities were preferred because they give slightly better results in the fitting of the direct ionization cross sections.

Figure 4 shows the ratios of multiple- to single-ionization cross sections of Ar by 1-MeV F^- ions as a function of the final target charge state. Solid symbols are used for experimental data and open symbols for results obtained from fitting. For 1-MeV F^- projectiles, we have performed the fitting

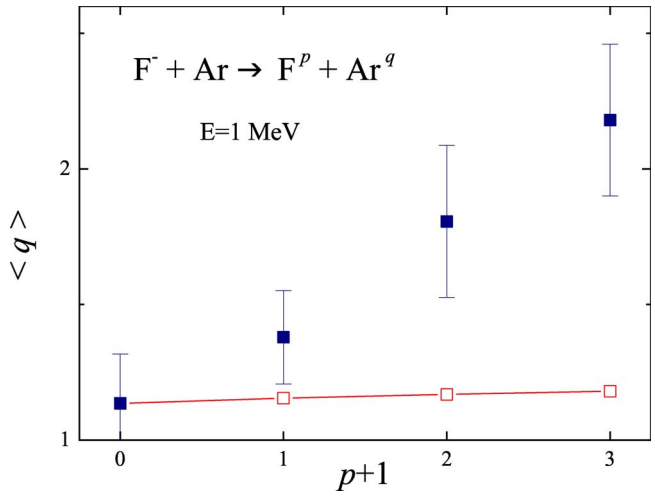

FIG. 5. (Color online) Average number of target electrons ionized, $\langle q \rangle$ [Eq. (10)], as a function of the projectile final charge state, $p+1$, for 1-MeV F^-+Ar collisions: solid squares, experimental data; open squares; results from fitting described in text.

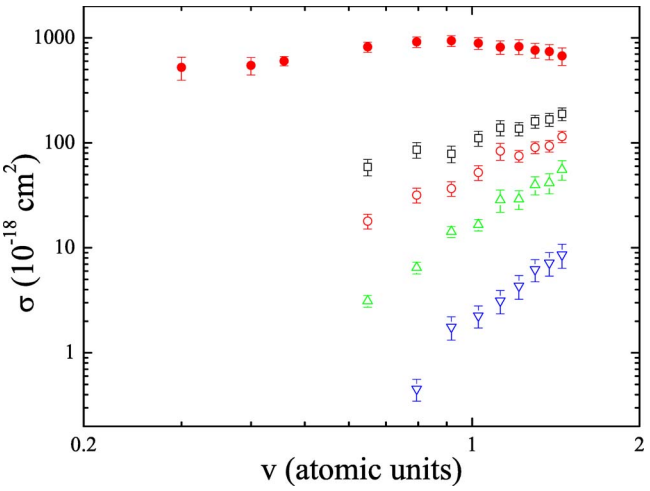

FIG. 6. (Color online) Cross sections for F^-+Ar projectile electron loss as a function of projectile velocity (this work, combined, for $q=0$, with data from Ref. [22]). For each target final charge state q, cross sections are summed over single-, double-, and triple-projectile-electron loss (p from 0 to 2): solid circles, projectile electron loss without target ionization ($q=0$); open squares, single ($q=1$); open circles, double ($q=2$); open triangles, triple ($q=3$); open down triangles, quadruple ($q=4$) target ionization.

procedure, adjusting the cross sections for target direct ionization (single, double, and triple) and total projectile direct ionization, using a least-squares method. Using Eqs. (6)–(9), fitted cross sections for all the measured collision channels are then determined. This approach works well for the direct-ionization channel, and the corresponding experimental data (solid squares) and fitted values (open squares) are indistinguishable in Fig. 4.

The measured ratios of multiple-to-single target ionization, for each q ($q=2$, 3, or 4, in Fig. 4), increases steeply with p (final projectile charge state). The ratios obtained from the fitting procedure also increase, but only slightly. Therefore, the correlation via impact parameter dependence is present but does not account for the high degree of correlation shown by the experimental data. Two-center electron-electron correlation, which was not taken into account in the binomial modeling, is a possible explanation for the enhancement in cross sections shown in Fig. 4. In order to highlight the limited role of correlation via impact parameter, we formally define the average $\langle q \rangle_{(p)}$ as

$$\langle q \rangle_{(p)} = \sum_q q \sigma^{p,q} \Big/ \sum_q \sigma^{p,q}, \tag{10}$$

with q running from 1 to 4, and plot, in Fig. 5, the values of $\langle q \rangle_{(p)}$ against the number of electrons lost by the projectile, $p+1$. Figure 5 shows that $\langle q \rangle_{(p)}$ increases with approximately uniform steps as the number of electrons lost by the projectile increases, for experimental data as well as for values extracted from fitting. However, the fitting values increase much slower, clearly outside the experimental error bars.

Our measurements cannot point clearly to a detailed model for the collision dynamics. However, Figs. 4 and 5 suggest that the electrons lost by the projectile can contribute to target multiple ionization, for example, by either (i) independently ionizing different target electrons or (ii) depositing together more energy than just one electron could do and therefore facilitating the ejection of several target electrons.

To gain further insight into the interaction between the projectile electrons and the target electrons we compare the projectile-electron-loss channels with and without target ionization. This latter collision channel is sometimes called *screening* projectile electron loss (or projectile elastic loss) since, in a simplified picture, the field of the target nucleus, screened by its electrons, ionizes the projectile with no target excitation or ionization [26,27].

When two-center electron-electron correlation plays a decisive role, projectile electron loss takes place with markedly different dynamics, sometimes called the *antiscreening* loss process. Here the projectile-electron–target-electron interaction is responsible for the projectile electron loss. The target electron is the ionizing agent of the projectile and, due to the energy and momentum transfer to the projectile, has a high probability of being ionized simultaneously with the projectile electron. Thus, coincidence measurements for projectile and target final charge states can, at least partially, determine experimentally the *antiscreening* cross section through the sum of cross sections $\sigma^{p,q}$ for which the target is ionized [30–32]. The interaction between projectile electrons results in a velocity threshold for the *antiscreening* process, like in the case of target ionization by electron impact [26,27]. There is, though, a softening of the velocity threshold when compared to the electron-projectile threshold, due to the momentum distribution of the projectile electrons.

Figure 6 shows F^-+Ar projectile total-electron-loss cross sections, for each target final charge state q, summed over single-, double-, and triple-projectile-electron loss (p from 0 to 2). Projectile total electron loss without target ionization [$q=0$, solid circles, data from this work combined with data from Ref. [22] according to Eq. (3)] clearly dominates electron loss over all studied velocity range. This result differs

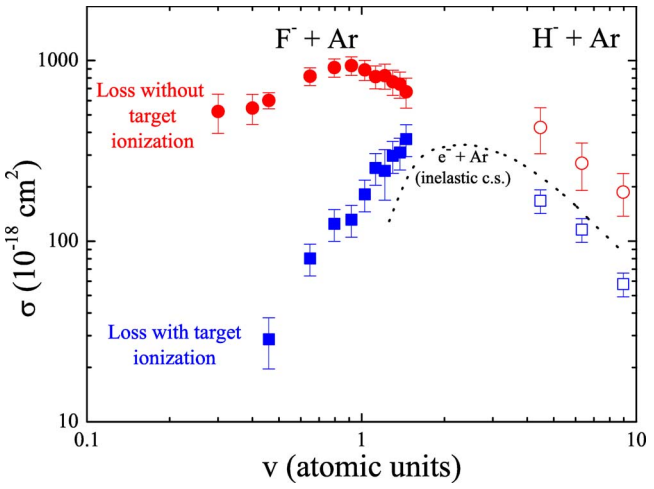

FIG. 7. (Color online) Cross sections for projectile electron loss as a function of projectile velocity. Projectile electron loss without target ionization: solid circles, F^-+Ar, this work combined with data from Ref. [22]; open circles, H^-+Ar, Ref. [10] combined with data from Ref. [34]. Projectile electron loss with target ionization: solid squares, F^-+Ar, this work; open squares, H^-+Ar [10]. Also shown are total inelastic cross sections for e^-+Ar [35].

from the case of positive projectiles, for which there is a strong coupling with the collision channel for electron capture by the projectile [33]. The velocity threshold shows up for all charged final target states except for $q=0$, consistently with the *screening-antiscreening* picture of projectile electron loss.

Figure 7 compares F^-+Ar projectile-electron-loss cross sections (summed over p from 0 to 2) for collision channels with target ionization (summed over q from 1 to 4, solid squares) and without target ionization ($q=0$, solid circles). The channel without target ionization corresponds to the *screening* mechanism (except for possible contributions from simultaneous projectile loss and target excitation, with posterior target fluorescent decay). This channel clearly dominates the total electron loss in the intermediate–to–low-velocity range. Figure 7 also shows high-velocity H^-+Ar projectile-electron-loss cross sections (summed over p from 0 to 1) for collision channels with target ionization (summed over q from 1 to 2, open squares) and without target ionization ($q=0$, open circles) (combining Refs. [10,34]). Total inelastic cross sections for electron impact are also shown [35]. The e^-+Ar data emphasize the softened threshold behavior of electron loss with target ionization. All the high-velocity data presented in Fig. 7 show the same velocity dependence. The high-velocity trend of projectile electron loss without target ionization is also consistent with the same dependence. There is obvious need of experimental and theoretical work, in the velocity gap between F^- and H^- data, in order to study the transition from the intermediate- to the high-velocity behavior of anion projectile electron loss.

IV. SUMMARY AND CONCLUSIONS

We have presented cross sections for single and multiple ionization of Ar by the anionic projectile F^-. Coincidence measurements using time-of-flight ion charge-state analysis allowed the determination of individual target ionization cross sections for single-, double-, and triple-projectile-electron loss and for direct target ionization. Our measurements are in the intermediate-velocity range, from 0.46 to 1.45 a.u. To our knowledge, the only other charge-state coincidence measurements available in the literature for an anion plus Ar collision system are high-velocity H^-+Ar data. Comparison between our F^- data and data for other projectiles (H^-, H^+, electrons, and antiprotons) incident on Ar gave insight into the mechanisms by which anion projectiles produce multiple ionization of an atomic target.

The role played by two-center electron-electron correlation is discussed and shown to be relevant for all the collision channels involving target ionization with simultaneous projectile ionization. For the direct ionization collision channels a simple independent-particle model is sufficient to describe the set of measured cross sections. For the projectile electron loss with target ionization, however, our data show that this is not the case. The high degree of two-center electron-electron correlation is highlighted in this work through analyzing the dependence of the average charge produced in the target as a function of the number of electrons lost by the projectile.

ACKNOWLEDGMENTS

This work was partially supported by the Brazilian agencies MCT/CNPq (CT-Energ), FINEP, CAPES, FAPERJ, and FUJB.

[1] T. Andersen, Phys. Rep. **394**, 157 (2004).
[2] D. J. Pegg, Rep. Prog. Phys. **67**, 857 (2004).
[3] T. Kirchner, A. C. F. Santos, H. Luna, M. M. Sant'Anna, W. S. Melo, G. M. Sigaud, and E. C. Montenegro, Phys. Rev. A **72**, 012707 (2005).
[4] O. Heber, G. Sampoll, B. B. Bandong, R. J. Maurer, R. L. Watson, I. Ben-Itzhak, J. M. Sanders, J. L. Shinpaugh, and P. Richard, Phys. Rev. A **52**, 4578 (1995).
[5] C. L. Cocke and R. E. Olson, Phys. Rep. **205**, 155 (1991).
[6] T. Tonuma, H. Shibata, S. H. Be, H. Kumagai, M. Kase, T. Kambara, I. Kohno, A. Ohsaki, and H. Tawara, Phys. Rev. A **33**, 3047 (1986).
[7] T. Tonuma, H. Kumagai, T. Matsuo, and H. Tawara, Phys. Rev. A **40**, 6238 (1989).
[8] T. Matsuo, T. Tonuma, H. Kumagai, and H. Tawara, Phys. Rev. A **50**, 1178 (1994).
[9] V. Shevelko and H. Tawara, *Atomic Multielectron Processes* (Springer-Verlag, Berlin, 1998).
[10] L. H. Andersen, L. B. Nielsen, and J. Sorensen, J. Phys. B **21**, 1587 (1988).

[11] F. Zappa, A. L. F. de Barros, L. F. S. Coelho, Ginette Jalbert, S. D. Magalhães, and N. V. de Castro Faria, Phys. Rev. A **70**, 034701 (2004).
[12] R. D. DuBois and S. T. Manson, Phys. Rev. A **35**, 2007 (1989).
[13] T. Spanger and T. Kirchner, J. Phys. B **37**, 4159 (2004).
[14] L. H. Andersen, P. Hvelplund, H. Knudsen, S. P. Moller, A. H. Sorensen, K. Elsener, K. G. Rensfelt, and E. Uggerhoj, Phys. Rev. A **36**, 3612 (1987).
[15] K. Paludan, H. Bluhme, H. Knudsen, U. Mikkelsen, S. P. Møller, E. Uggerhøj, and E. Morenzoni, J. Phys. B **30**, 3951 (1997). Data tables in http://www.ifa.au.dk/amo/collwap/leardata.htm
[16] J. D. Sherman and Y. I. Belchenko (Eds.), in *Production and Neutralization of Negative Ions and Beams*, AIP Conf. Proc. (AIP, Melville, NY, 2005).
[17] L. R. Grisham, Nucl. Instrum. Methods Phys. Res. A **464**, 315 (2001).
[18] L. R. Grisham, Fusion Sci. Technol. **43**, 191 (2003).
[19] M. M. Sant'Anna, F. Zappa, A. C. F. Santos, A. L. F. Barros, W. Wolf, L. F. S. Coelho, and N. V. de Castro Faria, Plasma Phys. Controlled Fusion **46**, 1009 (2004).
[20] J. Poulsen, T. Andersen, R. D. Cowan, P. Dahl, J. E. Hansen, and J. E. Pedersen, J. Phys. B **23**, 457 (1990).
[21] J. P. Grouard, V. A. Esaulov, R. I. Hall, J. L. Montmagnon, and Vu Ngoc Tuan, J. Phys. B **19**, 1483 (1986).
[22] F. Zappa, Ginette Jalbert, L. F. S. Coelho, A. B. Rocha, S. D. Magalhães, and N. V. de Castro Faria, Phys. Rev. A **69**, 012703 (2004).
[23] R. D. DuBois, L. H. Toburen, and M. E. Rudd, Phys. Rev. A **29**, 70 (1984).
[24] A. C. F. Santos, Ph.D. thesis, Catholic University of Rio de Janeiro, 1999; A. C. F. Santos *et al.* (unpublished).
[25] R. C. Wetzel, F. A. Baiocchi, T. R. Hayes, and R. S. Freund, Phys. Rev. A **35**, 559 (1987).
[26] J. H. McGuire, *Electron Correlation Dynamics in Atomic Collisions* (Cambridge University Press, Cambridge, England, 1997).
[27] E. C. Montenegro, J. H. Mcguire, and W. E. Meyerhof, Adv. At., Mol., Opt. Phys. **29**, 217 (1992).
[28] T. J. Gray, C. L. Cocke, and E. Justiniano, Phys. Rev. A **22**, 849 (1980).
[29] C. F. Fisher, *The Hartree-Fock Method for Atoms* (Wiley, New York, 1977).
[30] E. C. Montenegro, W. S. Melo, W. E. Meyerhof, and A. G. dePinho, Phys. Rev. Lett. **69**, 3033 (1992).
[31] E. C. Montenegro, W. S. Melo, W. E. Meyerhof, and A. G. dePinho, Phys. Rev. A **48**, 4259 (1993).
[32] E. C. Montenegro, A. C. F. Santos, W. S. Melo, M. M. Sant'Anna, and G. M. Sigaud, Phys. Rev. Lett. **88**, 013201 (2001).
[33] M. M. Sant'Anna, Braz. J. Phys. **36**, 518 (2006).
[34] Y. Nakai, T. Shirai, T. Tabata, and R. Ito, At. Data Nucl. Data Tables **37**, 69 (1987).
[35] F. J. de Heer, R. H. J. Jansen, and W. van der Kaay, J. Phys. B **12**, 979 (1979).